

A Simple Boundary Condition Regularization Strategy for Image Velocimetry Based Pressure Field Reconstruction

Connor Pryce¹, Lanyu Li¹, Jared P. Whitehead², and Zhao Pan^{*1}

¹University of Waterloo, Dept. of Mechanical and Mechatronics Engineering, Waterloo, ON, Canada

²Brigham Young University, Mathematical Dept., Provo, UT, USA

February 20, 2024

Abstract

We propose a simple boundary condition regularization strategy to reduce error propagation in pressure field reconstruction from corrupted image velocimetry data. The core idea is to replace the canonical Neumann boundary conditions with Dirichlet ones obtained by integrating the tangential part of the pressure gradient along the boundaries. Rigorous analysis and numerical experiments justify the effectiveness of this regularization.

1 Background and Statement of the Problem

Solving the Pressure Poisson Equation (PPE) is one popular approach to pressure field reconstruction from image velocimetry data (Van Oudheusden, 2013). Techniques like Particle Image Velocimetry (PIV) and Lagrangian Particle Tracking (LPT) provide a non-intrusive estimate of the pressure gradient $\nabla p = \mathbf{g}(\mathbf{u}) = -\mathbf{u}_t - (\mathbf{u} \cdot \nabla)\mathbf{u} + \text{Re}^{-1}\nabla^2\mathbf{u}$ in the domain and on the boundary via the momentum equations, where \mathbf{g} is a function of the velocity field \mathbf{u} , and Re is the Reynolds number.

Applying the divergence to ∇p yields the PPE:

$$\nabla^2 p = f(\mathbf{u}) = -\nabla \cdot \left(\frac{\partial \mathbf{u}}{\partial t} + (\mathbf{u} \cdot \nabla)\mathbf{u} - \frac{1}{\text{Re}}\nabla^2\mathbf{u} \right), \quad (1)$$

where f is the data of the Poisson equation. To solve (1), boundary conditions are required. Commonly used boundary conditions are i) Dirichlet boundary conditions

$$p = h \quad \text{on } \partial\Omega, \quad (2)$$

which define the value of the pressure on the boundaries and are often measured by pressure transducers and/or estimated using Bernoulli's principle in irrotational regions of the domain (De Kat and Van Oudheusden, 2012); as well as ii) Neumann boundary conditions

$$\mathbf{n} \cdot \nabla p = g_n \quad \text{on } \partial\Omega, \quad (3)$$

*To whom correspondence may be addressed: zhao.pan@uwaterloo.ca

which define the pressure gradient normal to the boundary (\mathbf{n} is the outward pointing unit normal vector on the boundary $\partial\Omega$), and are often derived from the momentum equations.

While the Poisson equation benefits from the well-posedness of elliptic equations, superior numerical stability, ease of implementation, and high computational efficiency, experimentation (Charonko et al. (2010); Sperotto et al. (2022); Zhang et al. (2022)) has shown that pressure field reconstruction on a domain with long Neumann boundaries may suffer from excessive error propagation due to contaminated image velocimetry data. This observation is expected, and supported analytically for two reasons: i) locally, the error in the data near a Neumann boundary is amplified and ‘diffuses’ further into the interior of the domain (Faiella et al., 2021); and ii) globally, long Neumann boundaries result in a larger Poincare constant for the Laplacian operator and thus the error in the data may be further intensified when compared to a domain with Dirichlet conditions of the same length. For these reasons, and despite being available everywhere, Neumann boundary conditions should be avoided if possible (Pan et al., 2016). Alternatively, Dirichlet conditions are favourable for taming error propagation, but they are not always easily accessible in practice.

This renders a fundamental dilemma that inhibits the performance of the PPE for pressure field reconstruction from noisy velocimetry data. In an attempt to break this bottleneck, one idea is to replace the Neumann boundary conditions with derived Dirichlet ones. In this letter, we introduce a simple regularization strategy of this type to address the boundary condition dilemma, and provide a rigorous analysis and validation to show that this specific regularization can improve the quality of the pressure field reconstruction.

2 Boundary Condition Regularization

In addition to the natural choice of the canonical Neumann boundary conditions (cNBC) in (3), the momentum equations also provide the pressure gradient tangential to the boundary:

$$\boldsymbol{\tau} \cdot \nabla p = g_\tau \quad \text{on } \partial\Omega, \quad (4)$$

where g_τ is the pressure gradient projected on $\boldsymbol{\tau}$, the unit vector tangential to the boundary in the counter-clockwise direction. Assigning a reference pressure p_0 at a location ξ_0 on the boundary and integrating (4) directly gives the value of the pressure which is a derived Dirichlet boundary condition (dDBC):

$$p(\xi) = h_d = \int_{\xi_0}^{\xi} \boldsymbol{\tau} \cdot \nabla p dS + p_0 = \int_{\xi_0}^{\xi} g_\tau dS + p_0 \quad \text{on } \partial\Omega. \quad (5)$$

Using this dDBC to replace the canonical Neumann boundary conditions for the Poisson equation yields a Dirichlet problem.

3 Analysis and Error Estimate

We consider a simple example to see how the regularization strategy proposed in Sect. 2 can improve the performance of the pressure field reconstruction based on a PPE with only a single point Dirichlet condition provided on the boundary. The error-contaminated problem for a domain with cNBC can be described as

$$\nabla^2 \tilde{p} = \tilde{f} \quad \text{in } \Omega \quad (6a)$$

$$\mathbf{n} \cdot \nabla \tilde{p} = \tilde{g}_n \quad \text{on } \partial\Omega, \quad (6b)$$

where $\tilde{p} = p + \epsilon_p$, $\tilde{f} = f + \epsilon_f$, and $\tilde{g}_n = g_n + \epsilon_{g_n}$ are the contaminated pressure, data, and cNBC, respectively; and ϵ_p , ϵ_f , and ϵ_{g_n} are the corresponding error. Comparing (6) with (3) and (1) leads to a new Poisson equation with respect to the error in the pressure field:

$$\begin{aligned} \nabla^2 \epsilon_p &= \epsilon_f & \text{in } \Omega & \quad (7a) \\ \mathbf{n} \cdot \nabla \epsilon_p &= \epsilon_{g_n} & \text{on } \partial\Omega, & \quad (7b) \end{aligned}$$

For the error propagation problem of (7), if we measure ϵ_p with a space-averaged error ($\|\epsilon_p\|_{L^2\Omega} = \sqrt{\int \epsilon_p^2 d\Omega / |\Omega|}$), the techniques in Pan et al. (2016) provide an estimate for the error in the pressure field which we present here for convenience:

$$\|\epsilon_p\|_{L^2(\Omega)} \leq C_N \|\epsilon_f\|_{L^2(\Omega)} + D_N \|\epsilon_{g_n}\|_{L^2(\partial\Omega)}, \quad (8)$$

where $D_N = \sqrt{C_N C_{NB} |\partial\Omega| / |\Omega|}$ is the coefficient corresponding to the error contribution from the boundary. C_N and C_{NB} are the Poincare constants for the problem, independent of the image velocimetry technique, solver implementation and spatial resolution. These constants are solely determined by the geometry (i.e., shape, size, and dimension) of the domain and the setup of the boundary conditions. $|\partial\Omega|$, $|\Omega|$ represent the size (length, area, or volume, depending on the dimension of the problem) of the boundary and the domain.

If we apply the boundary regularization strategy described in Sect. 2, the error contaminated dDBC and the corresponding error are:

$$\begin{aligned} \tilde{p} &= \tilde{h}_d & \text{on } \partial\Omega & \quad (9a) \\ \epsilon_p &= \epsilon_{h_d} & \text{on } \partial\Omega, & \quad (9b) \end{aligned}$$

where ϵ_{h_d} is the error in the dDBC. Replacing (6b) with (9a), the Poisson problem (6a) is regularized, and the corresponding error propagation can be modeled by replacing (7b) with (9b) in (7). Similar techniques in Pan et al. (2016) provide an error estimate of the recovered pressure for a Dirichlet problem:

$$\|\epsilon_p\|_{L^2(\Omega)} \leq C_D \|\epsilon_f\|_{L^2(\Omega)} + \|\epsilon_{h_d}\|_{L^\infty(\partial\Omega)}, \quad (10)$$

where C_D is the corresponding Poincare constant. Noting that $|\epsilon_{h_d}| \leq \int_{\xi_0}^{\xi} |\epsilon_{g_\tau}| dS \leq |\partial\Omega| \|\epsilon_{g_\tau}\|_{L^2(\partial\Omega)}$, by the Cauchy-Schwarz inequality, $\|\epsilon_{h_d}\|_{L^\infty(\partial\Omega)}$ in (10) can be estimated as

$$\|\epsilon_{h_d}\|_{L^\infty(\partial\Omega)} \leq |\partial\Omega| \|\epsilon_{g_\tau}\|_{L^2(\partial\Omega)}. \quad (11)$$

Combining (10) and (11), we arrive at

$$\|\epsilon_p\|_{L^2(\Omega)} \leq C_D \|\epsilon_f\|_{L^2(\Omega)} + |\partial\Omega| \|\epsilon_{g_\tau}\|_{L^2(\partial\Omega)}, \quad (12)$$

which is an estimate of the error in the reconstructed pressure field when the regularization described in (5) is practiced. For a domain with a given geometry, the Poincare constant (C_D in (12)) is almost always smaller than that of the original Neumann problem (C_N in (8)). This suggests that the proposed regularization in (5) can improve the accuracy of the pressure reconstruction, especially for large domains.

Letting $\Omega = L \times L$ be a two-dimensional domain, a concrete example is presented to demonstrate the effectiveness of the proposed regularization. For the problem equipped with cNBC, (8) becomes:

$$\|\epsilon_p\|_{L^2(\Omega)} \leq \frac{L^2}{\pi^2} \|\epsilon_f\|_{L^2(\Omega)} + \frac{4}{\pi^{3/2}} L \|\epsilon_{g_n}\|_{L^2(\partial\Omega)}, \quad (13)$$

where $C_N = L^2/\pi^2$, $C_{NB} = 4L$, $|\Omega| = L^2$, and $|\partial\Omega| = 4L$. For the regularized problem on the same domain with dDBC, (12) turns into

$$\|\epsilon_p\|_{L^2(\Omega)} \leq \frac{L^2}{2\pi^2} \|\epsilon_f\|_{L^2(\Omega)} + 4L \|\epsilon_{g_\tau}\|_{L^2(\partial\Omega)}, \quad (14)$$

where $C_D = L^2/2\pi^2$. Comparing (13) against (14), it is obvious that the proposed regularization can produce a more accurate pressure reconstruction. For a square domain, C_D is half of C_N , and an elongated rectangular domain reduces this factor again, further taming error propagation. This is achieved at the potential cost of slightly increasing the impact of the error in the pressure gradient on the boundary (the constant $4L/\pi^{3/2}$ in front of $\|\epsilon_{g_n}\|_{L^2(\partial\Omega)}$ in (13) is smaller than the constant $4L$ in front of $\|\epsilon_{g_\tau}\|_{L^2(\partial\Omega)}$ in (14)). Thus, for experiments with high uncertainty in a large domain, the regularization is expected to be effective in reducing the error in the reconstructed pressure field.

4 Curl-Free Regularization on a Closed Boundary

If the regularization proposed in (5) is employed on a closed boundary, it may lead to a non-physical Dirichlet condition when the error on the boundary (ϵ_{g_τ}) is not curl-free. That is, after the integration indicated in (5), the pressure value at $\xi = \xi_0$ may not be continuous ($p(\xi_0^+) \neq p(\xi_0^-)$). If integrated along another direction starting from the same reference point and reference pressure, a different pressure along the boundary is expected. This should not be the case since ∇p is curl-free (including the path along the boundary), and integration on ∇p should be path-independent. To resolve this issue, we construct a continuous function $p(\xi)$ on the boundary such that $\nabla p(\xi)$ is an interpolant or regression of \tilde{g}_τ , subject to the constraint $p(\xi_0^+) = p(\xi_0^-) = p_0$.

In 2D, one way to explicitly achieve such a Dirichlet boundary is by linear interpolation:

$$p(\xi) = \tilde{h}_d = \underbrace{(1 - \theta) \int_{\xi_0}^{\xi} \boldsymbol{\tau} \cdot \nabla \tilde{p} dS}_{\text{counter clockwise int.}} + \underbrace{\theta \int_{\xi_0 + |\partial\Omega|}^{\xi} \boldsymbol{\tau} \cdot \nabla \tilde{p} dS}_{\text{clockwise int.}} + p_0, \quad (15)$$

where $\theta = (\xi - \xi_0)/|\partial\Omega|$, and $\xi_0 \leq \xi \leq \xi_0 + |\partial\Omega|$. Equation (15) has an apparent physical meaning and can be thought of as a weighted average of integration of $\nabla \tilde{p}$ along two different directions, with θ being a weighting parameter. For $\theta = 0$ or 1, the counter-clockwise or the clockwise integral starting from ξ_0 has not yet accumulated any error, and thus, $p(\xi_0^+) = p(\xi_0^-) = p_0$. When $\theta \in (0, 1)$, (15) is a linear interpolation between the two integrals, and it is easy to verify that $p'(\xi) = \boldsymbol{\tau} \cdot \nabla \tilde{p} = \tilde{g}_\tau$. This modified regularization guarantees that the resulting \tilde{h}_d is continuous even if the contaminated pressure gradient on the boundary is not curl-free, and thus this regularization can be considered as a curl-free boundary correction. Note, (15) is one of the simplest solutions, but not necessarily the only one or the best one; nevertheless, its advantage will be demonstrated in Sect. 5.

5 Numerical Experiments and Validation

To validate the proposed boundary regulation strategies proposed in (5) and (15), a synthetic flow based on the Taylor vortex contaminated by artificial error is considered numerically. The pressure field of the Taylor vortex is

$$p = -\frac{\rho H^2}{64\pi^2 \nu t^3} \exp\left(-\frac{r^2}{2\nu t}\right), \quad (16)$$

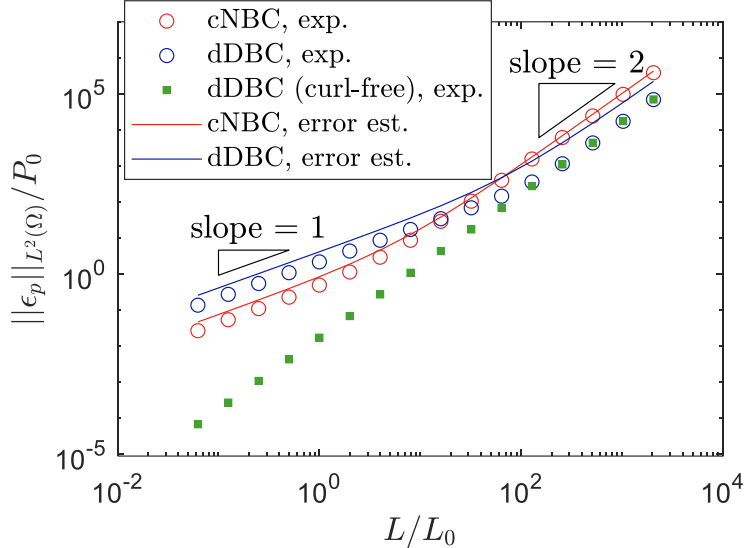


Figure 1: Error in the reconstructed pressure field ($\|\epsilon_p\|_{L^2(\Omega)}/P_0$) scaling with the length scale of the domain (L/L_0). Symbols represent the results from numerical experiments; the red and blue solid lines illustrate the error estimates indicated in (13) and (14), respectively.

where, H represents the angular moment of the vortex, ν the kinematic viscosity of the fluid, ρ the density of the fluid, t the time, and r the distance from the origin in polar coordinates. We choose the parameters so that the characteristic length scale of the vortex is $L_0 = \sqrt{2\nu t} = 1$ and the leading coefficient $\frac{\rho H^2}{64\pi^2 \nu t^3}$ as well as the amplitude of the characteristic pressure for this flow is unity ($P_0 = 1$). In this numerical experiment, the ground truth of the pressure field, the pressure gradients (i.e., g_n and g_τ) and the pressure Laplacian f are generated from (16) on an $L \times L$ square domain. Bias error (i.e., $\epsilon_{g_n} = 1$, $\epsilon_{g_\tau} = 1$ and $\epsilon_f = -1$) were added to the true solution to generate the synthetic data. This constant bias represents a global error with dominating low-frequency components and is typically challenging (Faiella et al., 2021). Using this synthetic data, the PPE was solved with the commonly used cNBC, the proposed dDBC, and the improved curl-free dDBC while varying the size of the domain. The reconstructed pressure was then compared to the ground truth to evaluate the error associated with each numerical experiment and is illustrated in Fig. 1.

As seen in Fig. 1, the results from the numerical experiments match the error estimates derived in Sect. 3 well. For the cNBC setup, the error estimate in (13) is relatively sharp, while the upper bound in (14) is slightly more conservative for the dDBC setup, meaning that the actual performance of the pressure solver with dDBC regularization is even better than expected. Both error estimates reveal the scaling behavior of the error in the pressure with the length scale of the domain L . For the two-dimensional cases, when the domain is large, the error in the domain (ϵ_f) dominates and $\|\epsilon_p\|_{L^2(\Omega)} \sim L^2$; while for a small domain, error on the boundary (ϵ_{g_n} or ϵ_{g_τ}) dominates and $\|\epsilon_p\|_{L^2(\Omega)} \sim L^1$. The curl-free dDBC proposed in Sect. 4 also performs as expected, resulting in even less error than the two aforementioned methods, especially when the domain is small. This test showcases the power of these simple regularization strategies and validates the error estimates outlined in Sect. 3.

The proposed boundary regularization strategies are further tested using synthetic data of a wake behind a cylinder with $Re = 100$, based on free stream velocity $U_\infty = 1$. A cropped and down-sampled high-fidelity simulation of the wake flow was used as the ground truth of the velocity and pressure fields. The cylinder of diameter D was centered at $(x/D, y/D) = (0, 0)$, and the cropped

domain is $(x/D, y/D) \in [2, 6] \times [-4, 4]$. The non-dimensional spatial and temporal resolution of the down-sampled data is $dx/D = dy/D = 0.0625$ and $dtD/U_\infty = 0.1$ respectively. Point-wise Gaussian noise with a variance equal to 1% of the magnitude of the free stream velocity was added to the ground truth velocity to generate the synthetic data. We reconstruct the pressure field using a second-order finite difference Poisson solver using the artificially contaminated velocity data and one point reference pressure at the bottom left corner of the domain $(x/D, y/D) = (2, -4)$ with cNBC, dDBC, and curl-free dDBC. The reconstructed pressure and the error are normalized by $P_0 = \frac{1}{2}\rho U_\infty^2$. 500 independent tests were carried out and depicted in Fig. 2.

The statistical tests in Fig. 2 show the performance of the three different boundary conditions with both the dDBCs performing much better than the cNBC as expected. In particular, the median error in the dDBC is reduced by roughly a factor of 10 when compared to the cNBC, and the curl-free dDBC reduces this error by an additional factor of ~ 2 . This is consistent with i) the theory that an elongated rectangular domain can reduce error propagation even further when compared to a square domain as indicated by (13) and (14); and ii) that the error estimate in (12) is rather conservative. In addition to greatly reducing the expected error in pressure (i.e., the mean of $\|\epsilon_p\|_{L^2(\Omega)}/P_0$ in Fig. 2(e) are 1.83, 0.17, and 0.11 for cNBC, dDBC, and curl-free dDBC case, respectively), the variance of $\|\epsilon_p\|_{L^2(\Omega)}/P_0$ is also reduced by the boundary regularization (e.g., the standard deviation of $\|\epsilon_p\|_{L^2(\Omega)}/P_0$ are 1.27, 0.10, and 0.05, cNBC, dDBC, and curl-free dDBC cases, respectively). This means that the proposed boundary regularization can improve both the accuracy and precision of pressure reconstruction. The observation in this test can also be explained from the numerical perspective: The resulting discretized systems from the PPE (i.e., $\mathcal{L}p = f$, where \mathcal{L} is the discretized Laplacian with associated boundary conditions) have 2-norm condition numbers of 1.1×10^4 and 4.6×10^5 with and without regularization, respectively, meaning that the regularization improves the numerical conditioning of the problem as well. The effectiveness of the boundary regularization can be directly visualized by Fig. 2(b–d) or Fig. 2(f–h), which is a typical case out of the 500 tests. Without boundary regularization, high bias in the reconstructed pressure (\tilde{p}) occurs due to the application of long Neumann boundaries, except for the bottom left corner where a transducer provides an accurate reference pressure (see Fig. 2(b&f)). From Fig. 2(c&g), it is obvious that replacing long cNBC with dDBC can effectively tame the error propagation; however, error accumulating along the boundary due to the practice of the regularization of (5) in the counter-clockwise direction is propagated to the interior of the domain (i.e., the ϵ_p is higher along the left edge of the domain than that of the bottom edge). This artifact is resolved by the curl-free dDBC regularization (see Fig. 2(d&h)). This suggests that even the curl-free correction on the boundary alone typically results in further reduction in ϵ_p throughout the entire domain.

6 Concluding Remarks and Perspectives

This work portrays a simple yet overlooked idea to regularize the velocity-based pressure field reconstruction: replacing the canonical Neumann boundary conditions with the Dirichlet conditions derived from integrating the tangential part of the pressure gradient on the boundary. This simple practice can effectively improve the quality, in terms of accuracy and robustness, of the pressure field reconstruction from corrupted image velocimetry data, which is analytically proved and validated by numerical experiments. The corresponding error estimates provided in this work are conservative i.e. pessimistic, but still dictate the generic dynamics of error propagation.

The proposed regularization strategies are very simple, and presumably can make Dirichlet conditions available everywhere with low computational cost. This is attractive as the derived Dirichlet conditions provide a ‘stronger’ type (Faiella et al., 2021) of information on the boundary

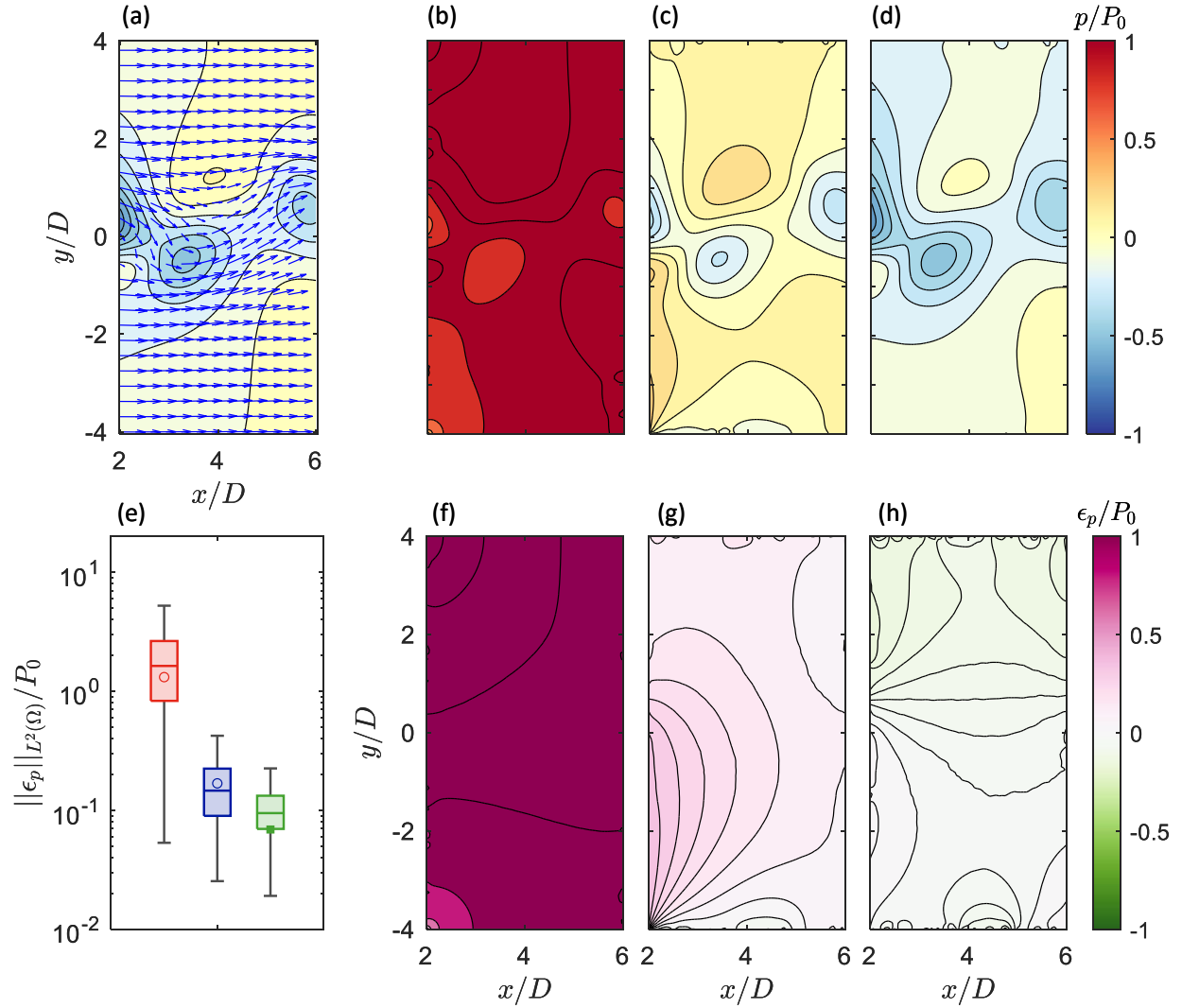


Figure 2: Typical results and statistical tests for pressure reconstruction with and without boundary regularization. (a) quiver plot of the velocity field overlaid on the pressure field ground truth; (b–d) reconstructed pressure field with cNBC, dDBC, and curl-free dDBC, respectively; (f–h) error in the reconstructed pressure field by comparing (b–d) with (a). (e) box plot of error in the pressure reconstruction from 500 independent tests with the red, blue, and green boxes corresponding to the statistics of the error for cNBC, dDBC, and curl-free dDBC cases, respectively. Horizontal bars in the middle of the boxes show the median while the upper and lower edges of the box indicate the 25 and 75 percentiles. The upper and lower whiskers bound the 95% confidence intervals of the error while the symbols within the boxes mark where the corresponding error shown in (f–h) lie within the data.

than cNBC alone. This ‘additional’ information on the boundary provides great flexibility and potential for more sophisticated algorithms to further improve the reconstruction. Our analysis is independent of the dimension of the domain (2D or 3D), and the continuous setting of the analysis indicates that the strategy works for structured or unstructured data based on PIV or LPT. Beyond establishing this family of regularization strategies, fulfilling the full potential of this seemingly odd, yet effective idea, will be left for future investigations.

7 Acknowledgement

We thank the discussion with Drs. Fernando Zigunov and Grady Wright. This work is partially supported by the Natural Sciences and Engineering Research Council of Canada (NSERC) Discovery Grant (RGPIN-2020-04486), and the Undergraduate Research Assistantship (URA) program, University of Waterloo. J.P.W. was partially supported by NSF grant DMS-2206762.

References

- Charonko, J. J., King, C. V., Smith, B. L., and Vlachos, P. P. (2010). Assessment of pressure field calculations from particle image velocimetry measurements. *Measurement Science and Technology*, 21(10):105401.
- De Kat, R. and Van Oudheusden, B. (2012). Instantaneous planar pressure determination from PIV in turbulent flow. *Experiments in fluids*, 52(5):1089–1106.
- Faiella, M., Macmillan, C. G. J., Whitehead, J. P., and Pan, Z. (2021). Error propagation dynamics of velocimetry-based pressure field calculations (2): on the error profile. *Measurement Science and Technology*, 32(8):084005.
- Pan, Z., Whitehead, J., Thomson, S., and Truscott, T. (2016). Error propagation dynamics of piv-based pressure field calculations: How well does the pressure poisson solver perform inherently? *Measurement Science and Technology*, 27(8):084012.
- Sperotto, P., Pieraccini, S., and Mendez, M. A. (2022). A meshless method to compute pressure fields from image velocimetry. *Measurement Science and Technology*, 33(9):094005.
- Van Oudheusden, B. (2013). PIV-based pressure measurement. *Measurement Science and Technology*, 24(3):032001.
- Zhang, J., Bhattacharya, S., and Vlachos, P. P. (2022). Uncertainty of piv/ptv based eulerian pressure estimation using velocity uncertainty. *Measurement Science and Technology*, 33(6):065303.